Fluid moments and spectral diagnostics in global gyrokinetic simulations

A. Bottino[1], C. Wersal[2], P. Angelino [2], B. Scott[1], B.F. McMillan[3], L.Villard[2]

[1] *Max-Planck-Institut für Plasmaphysik, Boltzmannstrasse 2, EURATOM Association, D-85748 Garching, Germany*

[2]*Ecole Polytechnique Fédérale de Lausanne, Centre de Recherches en Physique des Plasmas, Association Euratom-Confédération Suisse, CH-1015 Lausanne, Switzerland*

[3] *Department of Physics, Warwick University, Coventry CV47AL, UK*

The theoretical understanding of mesoscale and microscale turbulence is required for developing a predictive capability of heat, particle and momentum transport in tokamaks and stellarators. Codes based on gyrokinetic theory are suitable tools for studying low-frequency fluctuations in magnetized plasmas held responsible for microscale turbulence. In particular, the global code ORB5 [1] solves the full-f gyrokinetic Vlasov equation using a particle-in-cell δf method: the fluctuating part of the distribution function, δf, is discretized using a population of numerical particles, called markers. Each marker is characterized by a position in the 5D phase-space and by a weight, carrying the information of the average value of δf in a small portion of the phase-space. The linearized field equations, the polarization equation and the parallel Ampère's law [3], are discretized using finite elements. In collisionless simulations, like the ones discussed in this paper, the dissipation necessary to assure entropy saturation and reach a steady state is provided either by a zonal flow residual preserving Krook-operator [4] or by a coarse-graining algorithm [2]. In the absence of sources, transport processes tend to relax density and temperature profiles. In ORB5, the heat source has the form of a Krook operator modified to be particle conserving [4]. This source term tends to readjust the temperature profile toward the background profile, however small profile variations are still allowed during the time evolution. In the following, we will make use of the following definitions:

$$\begin{aligned}
\text{radial heat flux} \quad Q_\mathrm{h} &\equiv \Big\langle \frac{1}{|\nabla\psi|}\int \mathrm{d}W \frac{1}{B_\parallel^*}\frac{1}{2}mv^2\delta f \frac{\mathrm{d}\psi}{\mathrm{d}t}\Big|_{\mathrm{ExB}} \Big\rangle \\
\text{effective heat diffusivity} \quad \chi &\equiv Q_\mathrm{h}/n\nabla T \\
\text{generalized vorticity,} \quad \Omega &\equiv -e\nabla_\perp\left(\sum_{\text{species}}\frac{mn_0}{eB^2}\right)\nabla_\perp\Phi = \sum_{\text{species}} e\delta n \\
\text{density fluctuation,} \quad \delta n &\equiv \int \mathrm{d}W\ \delta f \\
\text{temperature fluctuations,} \quad \delta T &\equiv \frac{1}{3}m\left[\int \mu B\mathrm{d}W\ \delta f + \int mv_\parallel^2\mathrm{d}W\ \delta f - \left(\int mv_\parallel \mathrm{d}W\ \delta f\right)^2\right]
\end{aligned}$$

where ψ is the poloidal magnetic flux, Φ is the electrostatic potential, $(\mathbf{R}, p_z, \mu)$ are the gyrocen-

ter coordinates with $\mu \equiv v_\perp^2/2B$, magnetic moment per unit mass, and $p_z \equiv mv_\parallel$ is the canonical parallel momentum, m and e are the species mass and charge and $\mathrm{d}W = 2\pi B_\parallel^* m^{-2} \mathrm{d}\mu \mathrm{d}p_z$, $B_\parallel^*$ is the variable part of the velocity space volume element. The generalized vorticity, expressed as a frequency, is $\Omega \simeq (eB/m_D)(n_e - Z_i n_i)/n_0$.

The work presented in this paper is based on a new set of 3D diagnostics implemented in ORB5, allowing for instantaneous measurements of electromagnetic potentials and relevant fluid quantities (density, temperature, vorticity) on a full resolution 3D spatial mesh, making a massive use of parallel I/O. The same set of diagnostics can be used for 3D data visualization. Those diagnostics have been successfully applied to the study of electrostatic ion temperature gradient (ITG) driven turbulence, focusing in particular on the convergence properties of the different spectra [5]. In this paper we have applied the new tool-box to trapped electron mode (TEM) turbulence and to the case of ITG driven turbulence in the presence of finite β effects in realistic tokamak simulations.

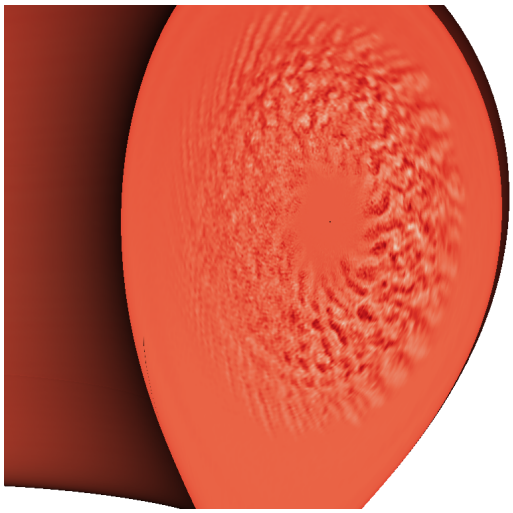

Figure 1: *Parallel magnetic potential, $A_{||}$, poloidal cross-section, $\beta_e = 0.3\%$.*

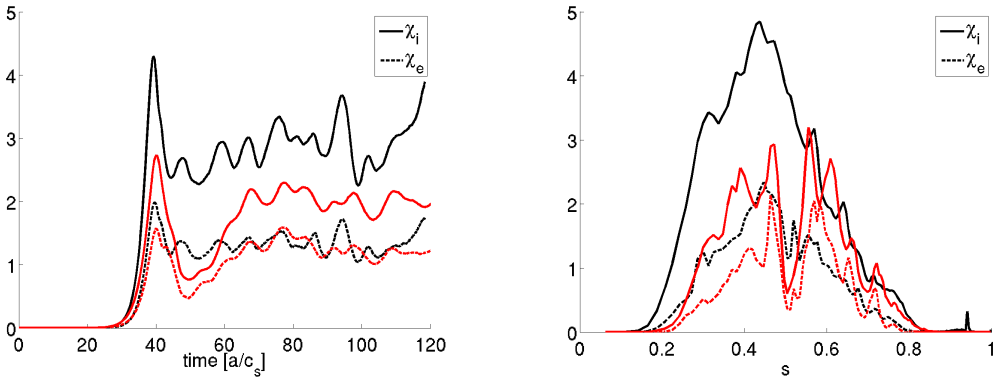

Figure 2: *Radial averaged, $[0.4 < s < 0.6]$, (left) and time averaged, $t > 60\ [a/c_s]$, (right) heat diffusivities for electrostatic, kinetic trapped electrons, (black) and EM, $\beta = 0.3\%$, (red) simulations.*

The magnetic equilibrium corresponds to the ASDEX Upgrade discharge #26754. Experimental density and temperature profiles have been modified in order to have a stronger gradient at mid-radius ($R/L_{Te} = R/L_{Ti} \simeq 7.5$). Two electrostatic simulations have been performed with different models for the electrons. In the first case, adiabatic electrons have been used, i.e. assuming $\delta n_e \simeq e n_0/T_{e0}(\phi - \bar{\phi})$, where $\bar{\phi}$ is the flux surface averaged electrostatic potential. In the

second case, only passing electrons are assumed to respond adiabatically to the potential perturbation while trapped electrons are treated kinetically (hybrid electron model). In addition to this, an electromagnetic (EM) simulation has been performed assuming $\beta_e \equiv \mu_0 n_e T_e / B^2 \simeq 0.3\%$ at mid-radius, comparable with the experimentally measured value of β_e. In all three cases, the dominant mode is an ITG further destabilized by trapped electrons. Figure 2 shows a comparison between the heat diffusivities of the EM (red) and the hybrid model (black) simulations. In both cases the ion heat diffusivity is higher than the electron one, consistent with ITG turbulence. However, EM effects significantly reduce the ion heat transport while keeping the electron channel almost unaffected. In this case, the mode is still an ITG but with a strong TEM component. The poloidal cross-section of the parallel magnetic potential is shown in Fig. 1. When fully adiabatic electrons are used, the ion heat diffusivity is a factor of two smaller than the kinetic trapped electron case.

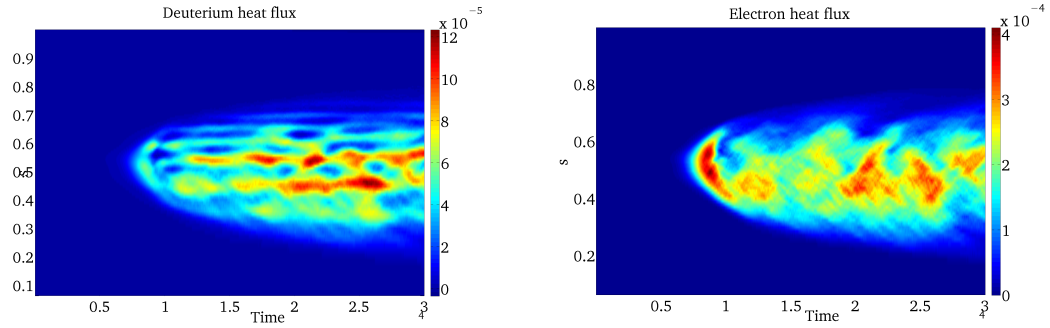

Figure 3: *Time evolution of the radial ion (left) and electron (right) heat fluxes, TEM case.*

Figure 3 shows the time evolution of the radial heat flux profiles for a simulation in which the dominant mode is a TEM. This was achieved by reducing the ion temperature gradient to values below the critical ITG threshold, i.e. $R/L_T \simeq 2.8$ at mid-radius. The heat flux evolution is characterized by several bursts and avalanches occurring intermittently in both in electron and ion channels. However, not only the electron heat flux is stronger than the ion one, as expected for TEM modes, but also it is only marginally affected by shearing effects due to zonal flows.

The 3D diagnostics allow for local and global fluctuation measurements and spectra. Figure 4 summarizes the behavior of the global density and temperature spectra time averaged over the steady state turbulence phase. Finite β effects and kinetic trapped electrons have little influence on the fluctuations spectra of ITG modes, despite their strong influence on the heat transport. TEM spectra peak at higher $k_\theta \rho_s$ than ITG spectra.

Finally, the scaling of the convergence in number of marker with the device size has been studied using the ITM-CYCLONE case [7], from small size tokamaks $\rho^{*-1} \simeq 92$ to ITER like machines $\rho^{*-1} \simeq 740$. For each value of $\rho*$, sources have been adjusted to keep the same

temperature profile during the saturation phase. Figure 5 (left) shows that the number of markers required for a given accuracy scales with ρ^{*2}, following the number of active modes present in the system, confirming the predictions of Ref. [8] for freely decaying turbulence. The spectra are self-similar for all the values of ρ^* considered here, an example of spectrum (vorticity) is illustrated in Fig. 5 (right).

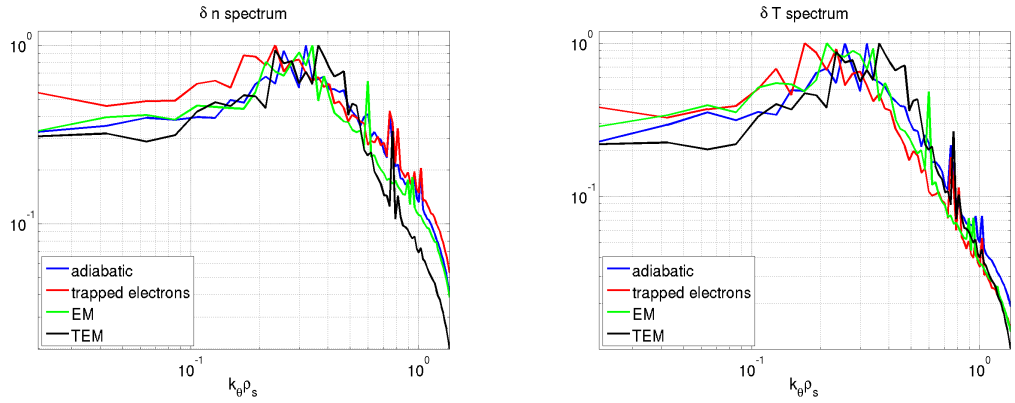

Figure 4: *Time and radial averaged density (left) and temperature (right) fluctuation spectra.*

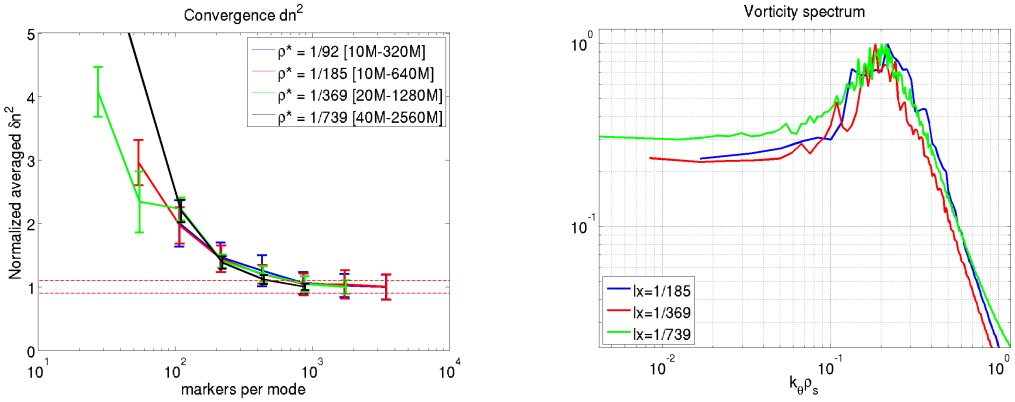

Figure 5: *Convergence in number of markers (left) and global vorticity spectrum (right) for different ρ^*, ITM-CYCLONE case.*

References

[1] S. Jolliet *et al.*, *Comput. Phys* **177**, 409 (2007)

[2] T. Vernay *et al.*, *Phys. Plasmas* **17**, 122301 (2010)

[3] A. Bottino *et al.*, *Plasma Phys. Controlled Fus.* **53**, 124027 (2011)

[4] B. F. McMillan *et al.*, *Phys. Plasmas* **16**, 022310 (2009)

[5] C. Wersal *et al.*, *Journ. Physics: Conf. Series* **401**, 012025 (2012)

[6] B. Scott *et al.*, *Phys. Plasmas* **17**, 112302 (2010)

[7] G. L. Falchetto *et al.*, *Plasma Phys. Controlled Fus.* **50**, 124015 (2008)

[8] A. Bottino *et al.*, *Phys. Plasmas* **14**, 010701 (2007)